

# First direct search for $2\epsilon$ and $\epsilon\beta^+$ decay of $^{144}\text{Sm}$ and $2\beta^-$ decay of $^{154}\text{Sm}$

P. Belli<sup>a,b</sup>, R. Bernabei<sup>a,b,1</sup>, R. S. Boiko<sup>c,d</sup>, F. Cappella<sup>e,f</sup>,  
V. Caracciolo<sup>a,b</sup>, R. Cerulli<sup>a,b</sup>, F. A. Danevich<sup>c</sup>, A. Di Marco<sup>a,b</sup>,  
A. Incicchitti<sup>e,f</sup>, B. N. Kropivnyansky<sup>c</sup>, M. Laubenstein<sup>g</sup>, S. Nisi<sup>g</sup>,  
D. V. Poda<sup>c,h</sup>, O. G. Polischuk<sup>c,b</sup> and V. I. Tretyak<sup>c</sup>

<sup>a</sup> INFN sezione Roma “Tor Vergata”, I-00133 Rome, Italy

<sup>b</sup> Dipartimento di Fisica, Università di Roma “Tor Vergata”, I-00133, Rome, Italy

<sup>c</sup> Institute for Nuclear Research, National Academy of Sciences of Ukraine, 03028 Kyiv, Ukraine

<sup>d</sup> National University of Life and Environmental Sciences of Ukraine, 03041 Kyiv, Ukraine

<sup>e</sup> INFN sezione Roma, I-00185 Rome, Italy

<sup>f</sup> Dipartimento di Fisica, Università di Roma “La Sapienza”, I-00185 Rome, Italy

<sup>g</sup> INFN, Laboratori Nazionali del Gran Sasso, I-67100 Assergi (AQ), Italy

<sup>h</sup> CSNSM, Univ. Paris-Sud, CNRS/IN2P3, Université Paris-Saclay, 91405 Orsay, France

## Abstract

The first direct search for the double electron capture ( $2\epsilon$ ) and the electron capture with positron emission ( $\epsilon\beta^+$ ) in  $^{144}\text{Sm}$  to the ground state and to the excited levels of  $^{144}\text{Nd}$  was realized by measuring – over 1899 h – a 342 g sample of highly purified samarium oxide ( $\text{Sm}_2\text{O}_3$ ) with the ultra-low background HP-Ge  $\gamma$  spectrometer GeCris (465 cm<sup>3</sup>) at the STELLA facility of the Gran Sasso National Laboratory (LNGS). No effect was observed and half-life limits were estimated at the level of  $T_{1/2} \sim (0.1 - 1.3) \times 10^{20}$  yr (90% C.L.). Moreover, for the first time half-life limits of the double beta ( $2\beta^-$ ) decay of  $^{154}\text{Sm}$  to several excited levels of  $^{154}\text{Gd}$  have been set; they are at the level of  $T_{1/2} \sim (0.06 - 8) \times 10^{20}$  yr (90% C.L.).

**Keywords:** Double beta decay;  $^{144}\text{Sm}$ ;  $^{154}\text{Sm}$ ; Low counting gamma spectrometry; Purification of samarium

---

<sup>1</sup>Corresponding author. *E-mail address:* rita.bernabei@roma2.infn.it.

# 1 Introduction

The studies on neutrino oscillations provide information about differences of squared neutrino masses, and show that the neutrino mass matrix of weak neutrino eigenstates is non-diagonal. In this theoretical framework, processes which can occur in the standard model (SM) are modified and other processes due to non vanishing neutrino masses can occur.

Double beta decay with neutrino emission conserves the lepton number, providing a confirmation of the SM of weak interaction. On the contrary, the neutrino-less double beta decay ( $0\nu2\beta$ ), which violates the lepton number by two units, can be a signature of new physics beyond the SM. Thus, investigations on neutrino-less double beta decay can provide information about neutrino properties, weak interaction, lepton number violation, and outline new theoretical frameworks [1–6]. While the two neutrino mode of double beta decay is already observed in several nuclides with the half-lives  $T_{1/2}^{2\nu2\beta} \sim 10^{18} - 10^{24}$  yr, for the  $0\nu2\beta$  decay the work is in progress. Typically, sensitivities on the half-life of the  $0\nu2\beta$  decay up to  $T_{1/2}^{0\nu2\beta} \geq 10^{24} - 10^{26}$  yr have been published with various kinds of experimental set-ups applying different procedures [5, 7–18]. Much more modest sensitivities have been presented in the investigations of the double beta plus processes ( $2\epsilon$ ,  $\epsilon\beta^+$  and  $2\beta^+$ ) [7, 19]. This could be ascribed e.g. to: (i) the technological progress in making detectors containing  $2\beta^-$  emitters, as e.g. germanium detectors; (ii) the typically larger abundance of the most promising  $2\beta^-$  emitters with respect to the  $2\beta^+$  emitters; (iii) the higher decay probability of  $2\beta^-$  processes with respect to that of the  $2\beta^+$  decay processes, which suffer of the suppression effect due to a smaller phase space factor. However, the investigations of  $\epsilon\beta^+$  and  $2\beta^+$  processes strongly contribute to clarify the mechanism of the  $0\nu2\beta^-$  decay [20]. Moreover, investigations of the  $0\nu2\epsilon$  processes are also supported by the possibility of a resonant enhancement of the capture rate because of the mass degeneracy between the initial and the final nucleus [21–27].

Experimental searches for  $2\nu2\beta$  processes, which are allowed in the SM and are already observed in dozen of nuclides [28] but not in Sm isotopes, give possibilities to check aspects of the theoretical calculations which are used also in the estimates of the half-lives of the  $0\nu2\beta$  mode.

In this paper the data collected with an ultra-low background (ULB) HP-Ge  $\gamma$  spectrometer have been analyzed in order to obtain new limits on double beta decay processes in  $^{144}\text{Sm}$  with emission of 511 keV  $\gamma$  quanta

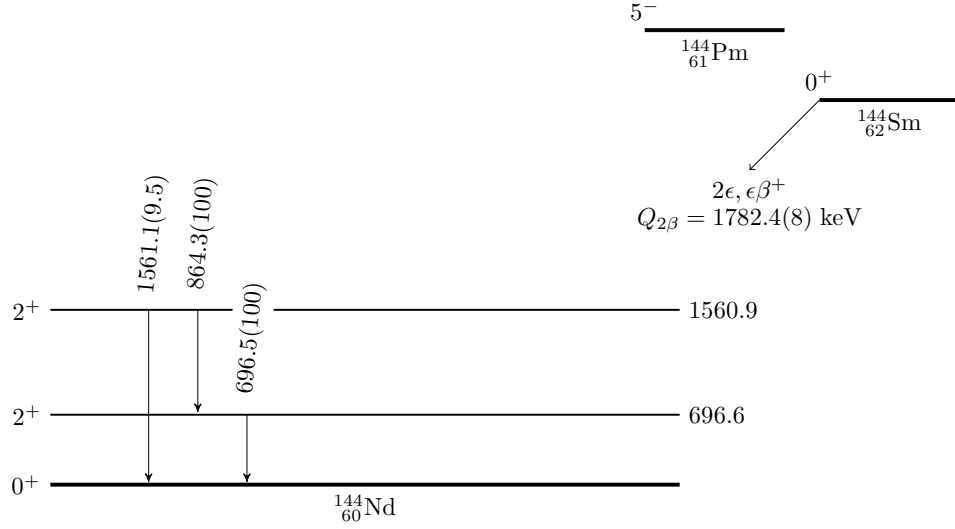


Figure 1: Simplified scheme of the double beta decay of  $^{144}\text{Sm}$  [29]. The energies of the excited levels and of the emitted  $\gamma$  quanta are in keV; the relative intensities of the  $\gamma$  quanta are given in parentheses.

after the  $\beta^+$  annihilation, or  $\gamma$  quanta expected in the de-excitation of the daughter nuclei. A simplified scheme of the double beta decay of  $^{144}\text{Sm}$  is presented in Fig. 1.

Moreover,  $^{154}\text{Sm}$   $2\beta^-$  decay is possible to the ground and to the several excited levels of  $^{154}\text{Gd}$  with subsequent emission of  $\gamma$  quanta with energies in the range (123 – 1059) keV (see Fig. 2). The characteristics of  $^{144}\text{Sm}$  and  $^{154}\text{Sm}$  isotopes are given in Table 1.

Table 1: Characteristics of the samarium isotopes candidates for what concerns double beta decay.

$2\beta$ Transition	$Q_{2\beta}$ (keV) [31]	Isotopic Abundance (%) [32]	Decay Channel [7]
$^{144}\text{Sm} \rightarrow ^{144}\text{Nd}$	1782.4(8)	3.08(4)	$\epsilon\beta^+$ , $2\epsilon$
$^{154}\text{Sm} \rightarrow ^{154}\text{Gd}$	1250.8(9)	22.74(14)	$2\beta^-$

The measurements with Sm are part of our program to investigate the possibility to purify lanthanide elements and, using the purified samples, to

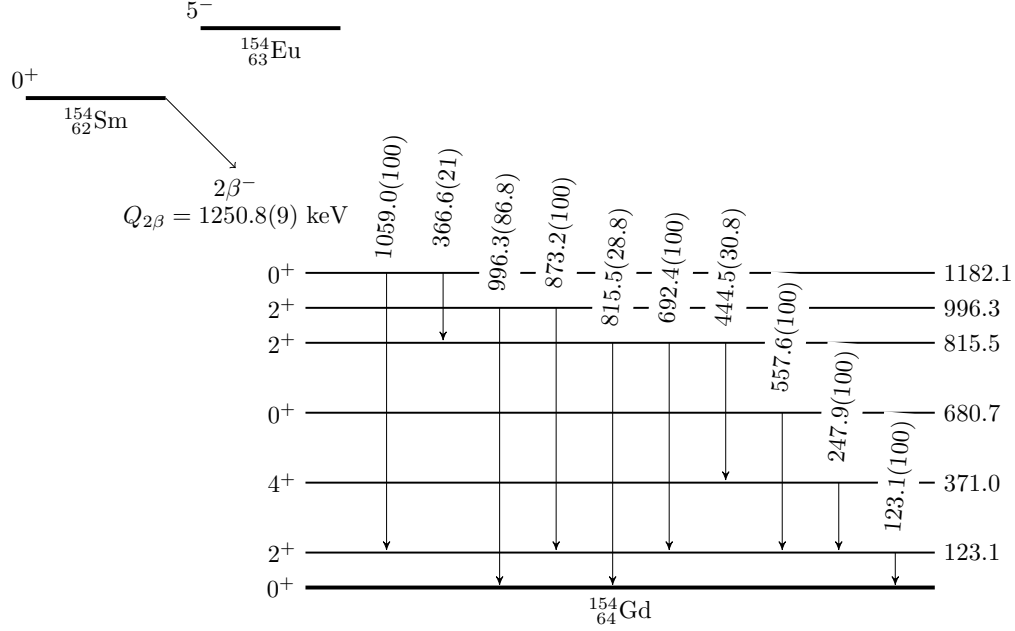


Figure 2: Simplified decay scheme of  $^{154}\text{Sm}$  [30]. The energies of the excited levels and of the emitted  $\gamma$  quanta are in keV; the relative intensities of the  $\gamma$  quanta are given in parentheses. Only energy levels and  $\gamma$  transitions with relative intensity larger than 3% are shown.

study the results of the purification and also to look for their  $2\beta$  processes in low-scale experiments [33–37]. The interest for purification is related mainly to  $^{150}\text{Nd}$  and  $^{160}\text{Gd}$ , also rare-earth nuclides, which are ones of the most promising candidates for  $0\nu 2\beta$  decay searches. Some details on purification can be found in [38].

To our knowledge, theoretical estimates of the half-lives for  $^{144}\text{Sm}$  are absent in the literature. The half-life for  $0\nu 2\epsilon$  mode (ground state to ground state, g.s. to g.s., transition) was calculated as  $1.0 \times 10^{31}$  yr [39]. The only known experimental limits were obtained only recently as  $8.0 \times 10^8$  yr for all the decay modes and  $1.0 \times 10^{15}$  yr the  $0\nu \epsilon \beta^+$  mode (g.s. to g.s.) [40]. For  $^{154}\text{Sm}$ , the theoretical results for neutrinoless mode are at level of  $10^{24} - 10^{26}$  yr (for g.s. to g., and neutrino mass of 1 eV) [41–44]. For the two neutrino decay of  $^{154}\text{Sm}$  (g.s. to g.s.), the theoretical results are at level of  $10^{20} - 10^{23}$  yr [41, 45–49]. The half-life for  $2\nu 2\beta$  decay of  $^{154}\text{Sm}$  to the level of  $^{154}\text{Gd}$

(123 keV) was calculated as  $1.4 \times 10^{29}$  yr [41] (it is rather long, in particular, due to the change in spin by 2 units). Experimental limit was set only for transition to  $2_1^+$  level (123 keV) as  $2.3 \times 10^{18}$  yr [50].

## 2 The experiment

### 2.1 The purification of samarium oxide

Commercially available samarium oxide  $\text{Sm}_2\text{O}_3$  from Stanford Materials Corporation ( $>99.5\%$  total rare earth oxide (TREO) and  $>99.999\%$  of  $\text{Sm}_2\text{O}_3/\text{TREO}$ ) was used as starting material. The sample was firstly measured by ICP-MS and by ULB HP-Ge  $\gamma$ -spectroscopy to determine the initial purity. The main radioactive contaminants of the material are radium, thorium, uranium and lutetium, typical impurities in the lanthanide elements [34, 51–54].

After those measurements, purification procedures have been applied; they consist of several stages of chemical and physical transformations: (i) dissolution of the initial oxide in nitric acid; (ii) fractional precipitation of the  $\text{Sm}(\text{OH})_3$ ; (iii) liquid-liquid extraction; (iv) complete precipitation of the  $\text{Sm}(\text{OH})_3$  and (v) samarium oxide recovery.

To prepare homogeneous aqueous solutions of samarium, diluted nitric acid (Alfa Aesar) was added to the suspension of  $\text{Sm}_2\text{O}_3$  in deionized water ( $18.2 \text{ M}\Omega \times \text{cm}$ ). The obtained solution was analysed and the concentrations determined as 1.58 M for  $\text{Yb}(\text{NO}_3)_3$  and 2.5 M for residual  $\text{HNO}_3$ , respectively.

After the first step, ammonia gas was added to the acidic solution to cause partial (fractional) precipitation of lanthanides. At the same time also impurities like Th, Fe hydroxides started to co-precipitate. This is possible since the hydroxides of thorium and iron precipitate at a lower pH level than Sm hydroxide. After this procedure the final pH of the solution was about 6.5 and the mass of the precipitated Sm was 3.4% of the initial mass. The obtained amorphous  $\text{Sm}(\text{OH})_3$  sediment was separated from the supernatant liquid by using a centrifuge, then annealed to  $\text{Sm}_2\text{O}_3$  and analysed by ICP-MS in order to determine the efficiency of the co-precipitation of the impurities (see Table 2). This part of samarium oxide was excluded from the further purification procedure.

The liquid-liquid extraction procedure was applied for the purification of the aqueous solution from uranium and thorium traces. In this stage

Table 2: Results of the ICP-MS analysis.

Element	Concentration (ppb)		
	Initial material	Sediment after fractional precipitation (waste)	Purified material
K	<2000	1639	424
Fe	2400	27441	1190
Th	2.2	9.5	<0.3
U	48	321	<0.1
Pb	90	466	56
La	1300	700	1200
Lu	6200	12700	4100

the solution was acidified with diluted nitric acid down to pH equal to 1. The tri-n-octylphosphine oxide (TOPO, 99%, Acros Organics) was used as organic complexing agent for binding U and Th, while toluene ( $\geq 99.7\%$ , ACS reagent, Sigma-Aldrich) was used as solvent liquor. Considering the very low concentration, the concentration of TOPO in toluene did not exceed 0.1 mol/l. Two immiscible liquids (aqueous solution and organic solution) were placed into a separation funnel in volumetric ratio 1:1 and shaken up for a few minutes. Uranium and thorium interact with TOPO forming organo-metallic complexes that have much higher solubility in the organic phase than in the water solution. This leads to extraction of U and Th into the organic liquid. After the separation of the purified aqueous solution, samarium was completely precipitated in form of hydroxide by adding ammonia gas. The obtained sediments were separated, dried and annealed at 900°C for a few hours. Finally, 342 g of purified Sm oxide were obtained.

## 2.2 The low counting experiment

The experiment was carried out at the STELLA facility of the LNGS by using the ULB HP-Ge detector “GeCris” with volume 465 cm<sup>3</sup>. The detector is shielded with low radioactivity lead ( $\sim 25$  cm), copper ( $\sim 5$  cm), and, in the inner-most part, with archaeological Roman lead ( $\sim 2.5$  cm). The set-up is placed in an air-tight poly-methyl-methacrylate box and flushed with high purity nitrogen gas to exclude the environmental radon. The purified sample

of  $\text{Sm}_2\text{O}_3$  with mass 342 g was enclosed in a cylindrical polystyrene box on the HP-Ge detector end cap.

The energy resolution of the detector was estimated by using background  $\gamma$ -ray peaks with energies 238.6 keV ( $^{212}\text{Pb}$ ), 338.3 keV ( $^{228}\text{Ac}$ ), 463.0 keV ( $^{228}\text{Ac}$ ), 583.2 keV ( $^{208}\text{Tl}$ ), 661.7 keV ( $^{137}\text{Cs}$ ), 727.3 keV ( $^{212}\text{Bi}$ ), 911.2 keV ( $^{228}\text{Ac}$ ), 1460.8 keV ( $^{40}\text{K}$ ) and 2614.5 keV ( $^{208}\text{Tl}$ ), measured in the contiguous experiment of Ref. [33] with a cerium oxide sample, and verified with the present  $\text{Sm}_2\text{O}_3$  data taking.

The energy resolution of the detector depends on the energy of the  $\gamma$  quanta,  $E_\gamma$ , according to:  $\text{FWHM}(\text{keV}) = \sqrt{1.41 + 1.97 \times 10^{-3} E_\gamma}$ , where  $E_\gamma$  is in keV. The data with the  $\text{Sm}_2\text{O}_3$  sample were taken over 1899 h, while the background spectrum was collected for 1046 h. The two spectra, normalized to the time of measurements, are presented in Fig. 3. Some excess of  $^{137}\text{Cs}$ ,  $^{138}\text{La}$ ,  $^{176}\text{Lu}$  and  $^{214}\text{Bi}$  (daughter of  $^{226}\text{Ra}$ ) with respect to the background data was observed; this allowed us to estimate the concentration of these radionuclides in the sample. The activities of the nuclides in the  $\text{Sm}_2\text{O}_3$  sample after its purification are also shown in Table 3. The concentration of  $^{176}\text{Lu}$  remained almost the same as prior to the purification<sup>2</sup>; this is due to the high chemical affinity between the Sm and Lu, both lanthanides, while the activity of  $^{226}\text{Ra}$  is decreased by a factor 4. The activities of  $^{228}\text{Th}$ ,  $^{228}\text{Ra}$ ,  $^{234m}\text{Pa}$  and  $^{235}\text{U}$  were reduced by about one order of magnitude (see Table 3).

### 2.3 The search for double beta decay processes

There are no peculiarities in the energy spectrum of the  $\text{Sm}_2\text{O}_3$  sample that could be identified as double beta decay of the Sm isotopes. Therefore, half-life limits of the  $\epsilon\beta^+$  and  $2\epsilon$  processes in  $^{144}\text{Sm}$  and of the  $2\beta^-$  processes in  $^{154}\text{Sm}$  were estimated. The lower half-life limits were calculated using the following equation:

$$T_{1/2,\text{lim}} = N \times \eta \times t \times \frac{\ln 2}{S_{\text{lim}}}, \quad (1)$$

where: i)  $N$  is the number of nuclei of interest in the sample; ii)  $\eta$  is the full energy peak (FEP) detection efficiency of  $\gamma$  quanta (including the  $\gamma$ -ray

---

<sup>2</sup>It is similar to what was observed in the purification of other rare earth elements, e.g. [34–36].

Table 3: Radioactive contaminations of the samarium oxide before and after applying the purification procedures as measured with the ultra-low background HP-Ge  $\gamma$  spectrometer. The upper limits are given at 95% confidence level (C.L.), and the uncertainties are  $1\sigma$ .

Chain	Nuclide	Activity (mBq/kg)	
		Before purification	After purification
	$^{40}\text{K}$	$< 11$	$11 \pm 5$
	$^{137}\text{Cs}$	$< 0.67$	$0.8 \pm 0.2$
	$^{138}\text{La}$	-	$0.81 \pm 0.16$
	$^{152}\text{Eu}$	-	$< 0.50$
	$^{154}\text{Eu}$	-	$< 0.43$
	$^{176}\text{Lu}$	$(0.23 \pm 0.02) \times 10^3$	$(0.203 \pm 0.015) \times 10^3$
$^{232}\text{Th}$	$^{228}\text{Ra}$	$11 \pm 2$	$1.4 \pm 0.7$
	$^{228}\text{Th}$	$24 \pm 3$	$< 1.1$
$^{238}\text{U}$	$^{234}\text{Th}$	$< 1.7 \times 10^3$	$< 0.13 \times 10^3$
	$^{234m}\text{Pa}$	$(0.22 \pm 0.05) \times 10^3$	$< 18$
	$^{226}\text{Ra}$	$6 \pm 1$	$1.5 \pm 0.4$
$^{235}\text{U}$	$^{235}\text{U}$	$31 \pm 7$	$< 2.7$
	$^{231}\text{Pa}$	-	$< 15$
	$^{227}\text{Th}$	-	$5 \pm 2$
	$^{223}\text{Ra}$	-	$< 10$
	$^{211}\text{Pb}$	-	$< 6.7$
	$^{207}\text{Tl}$	-	$< 52$



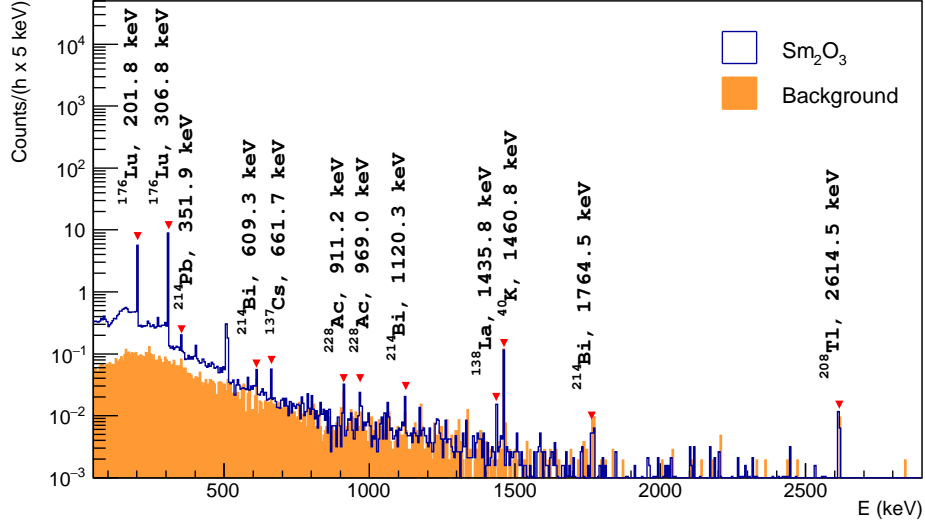


Figure 3: (Color online) Energy spectra measured by the ULB HP-Ge spectrometer with the  $\text{Sm}_2\text{O}_3$  sample over 1899 h ( $\text{Sm}_2\text{O}_3$ ) and without the sample over 1046 h (Background).

emission intensity); iii)  $t$  is the time of measurement; iv)  $S_{lim}$  is the upper limit on the number of events of the effect, searched for, that can be excluded at a given C.L.. In the present work all the  $S_{lim}$  values and, therefore, the half-life limits are given at 90% C.L. The detection efficiencies of the processes searched for were Monte-Carlo simulated by using the EGSnrc [53] package with initial kinematics given by the DECAY0 event generator [54]. The  $\text{Sm}_2\text{O}_3$  sample contained  $2.69 \times 10^{23}$  and  $3.64 \times 10^{22}$  nuclei of  $^{154}\text{Sm}$  and  $^{144}\text{Sm}$ , respectively.

## 2.4 The search for the $\epsilon\beta^+$ and the $2\epsilon$ processes in $^{144}\text{Sm}$

In the case of  $2\epsilon$  decays, a cascade of X-rays and Auger electrons is expected. Moreover, the double electron capture in  $^{144}\text{Sm}$  is also allowed to excited levels of  $^{144}\text{Nd}$  with subsequent emission of gamma quanta that can be detected with the HP-Ge spectrometer.

In order to estimate the limits on the  $2\nu 2\epsilon$  and  $0\nu 2\epsilon$  decays of  $^{144}\text{Sm}$  to the  $2^+$  excited levels of  $^{144}\text{Nd}$ , the energy spectrum of the  $\text{Sm}_2\text{O}_3$  sample was

fitted in the energy intervals where intense  $\gamma$ -ray peaks from the de-excitation process are expected. The limits obtained for the double electron capture of  $^{144}\text{Sm}$  to the excited levels of  $^{144}\text{Nd}$  are given in Table 4.

For the  $0\nu 2\epsilon$  decay mode of  $^{144}\text{Sm}$  to the ground and the excited levels of  $^{144}\text{Nd}$  only the captures from  $K$  and  $L$  shells were considered here; we assume that the energy excess is taken away by bremsstrahlung  $\gamma$  quanta with energy  $E_\gamma = Q_{2\beta} - E_{b1} - E_{b2} - E_{exc}$ , where  $E_{bi}$  are the binding energies of the captured electrons in the atomic shells of the daughter neodymium

Table 4: The half-life limits on the  $2\beta$  processes in  $^{144}\text{Sm}$  and  $^{154}\text{Sm}$ .

Process of decay	Decay mode	Level of daughter nucleus (keV)	$E_\gamma$ (keV)	FEP detection efficiency (%)	$S_{lim}$	Experimental limit (yr) at 90% C.L.
$^{144}\text{Sm} \rightarrow ^{144}\text{Nd}$						
$2K$	$2\nu$	$2^+$ 696.6	696.5	2.93	10	$\geq 1.6 \times 10^{19}$
$2K$	$2\nu$	$2^+$ 1560.9	864.3	2.14	0.90	$\geq 1.3 \times 10^{20}$
$\epsilon\beta^+$	$2\nu$	g.s.	511.0	6.55	10	$\geq 3.6 \times 10^{19}$
$\epsilon\beta^+$	$2\nu$	$2^+$ 696.6	511.0	5.76	10	$\geq 3.2 \times 10^{19}$
$2K$	$0\nu$	g.s.	1695.3	1.87	2.3	$\geq 4.4 \times 10^{19}$
$KL$	$0\nu$	g.s.	1731.7	1.84	6.0	$\geq 1.7 \times 10^{19}$
$2L$	$0\nu$	g.s.	1768.2	1.81	7.0	$\geq 1.4 \times 10^{19}$
$2K$	$0\nu$	$2^+$ 696.6	696.5	2.57	10	$\geq 1.4 \times 10^{19}$
$2K$	$0\nu$	$2^+$ 1560.9	864.3	2.08	0.90	$\geq 1.3 \times 10^{20}$
$\epsilon\beta^+$	$0\nu$	g.s.	511.0	6.38	10	$\geq 3.5 \times 10^{19}$
$\epsilon\beta^+$	$0\nu$	$2^+$ 696.6	511.0	5.77	10	$\geq 3.2 \times 10^{19}$
$^{154}\text{Sm} \rightarrow ^{154}\text{Gd}$						
$2\beta^-$	$2\nu+0\nu$	$2^+$ 123.1	123.1	0.40	27	$\geq 6.0 \times 10^{18}$
$2\beta^-$	$2\nu+0\nu$	$0^+$ 680.7	557.6	3.08	4.8	$\geq 2.6 \times 10^{20}$
$2\beta^-$	$2\nu+0\nu$	$2^+$ 815.5	692.4	1.80	2.4	$\geq 3.0 \times 10^{20}$
$2\beta^-$	$2\nu+0\nu$	$2^+$ 996.3	873.2	1.39	2.8	$\geq 2.0 \times 10^{20}$
$2\beta^-$	$2\nu+0\nu$	$0^+$ 1182.1	1059.0	1.99	1.0	$\geq 8.0 \times 10^{20}$

atom, and  $E_{exc}$  is the energy of the excited level.

In the case of  $2\nu 2K$  or  $0\nu 2K$  capture in  $^{144}\text{Sm}$  to the first ( $2^+$ , 696.6 keV) excited level,  $\gamma$  quanta with 696.5 keV energy are expected. The  $S_{lim}$  value was obtained by fitting the experimental data in the energy interval where the peak is expected, considering a linear background model plus a

Gaussian peak at 696.5 keV energy, taking into account the energy resolution described above. In the range (670–730) keV the fit provides the area of the peak searched for with  $\chi^2/n.d.f. \simeq 0.99$  (n.d.f. = number of degrees of freedom); it is:  $(3.1 \pm 4.3)$  counts, that is no evidence on the effect searched for. Thus, the  $S_{lim}$  value was estimated using the procedure of Ref. [55];  $S_{lim} = 10$  counts was obtained. The FEP detection efficiencies for the  $2\nu 2K$  and  $0\nu 2K$  modes, simulated by a dedicated Monte-Carlo code, were:  $\eta = 2.93\%$ ,  $\eta = 2.57\%$ , respectively. Taking into account the number of  $^{144}\text{Sm}$  nuclei in the sample, the half-life limits of Table 4 were obtained.

A similar procedure was followed to estimate the  $S_{lim}$  value for the 864.3 keV peak expected for the  $2\nu 2K$  and  $0\nu 2K$  transitions to the  $^{144}\text{Nd}$  1560.9 keV level. The fit, performed within the energy range (855–885) keV ( $\chi^2/n.d.f. \simeq 0.99$ ), gives  $(-1.1 \pm 1.1)$  counts; the  $S_{lim}$  value, estimated by applying the procedure of Ref. [55], was: 0.90 counts. The FEP detection efficiencies, simulated by Monte-Carlo code, are  $\eta = 2.14\%$  and  $2.08\%$ , respectively. The derived half-life limit in both cases is:  $T_{1/2} \geq 1.3 \times 10^{20}$  yr.

In the case of  $0\nu 2K$  capture in  $^{144}\text{Sm}$  to the  $^{144}\text{Nd}$  g.s., 1695.3 keV  $\gamma$  quanta are expected. Following the same procedure described above, the fit provides – in the (1670–1720) keV energy range ( $\chi^2/n.d.f. \simeq 0.30$ ) – an area for the  $0\nu 2K$  process equal to  $(0.0 \pm 1.4)$  counts. The  $S_{lim}$  value, estimated using the procedure of Ref. [55], was 2.3 counts. The FEP detection efficiency, simulated by Monte-Carlo code, was:  $\eta = 1.87\%$ . The half-life limit, obtained for this process, is  $T_{1/2} \geq 4.4 \times 10^{19}$  yr at 90% C.L.

In case of  $0\nu KL$  and  $0\nu 2L$  processes to the g.s. of  $^{144}\text{Nd}$  (see Fig. 4), the energies of the  $\gamma$  quanta are 1731.7 keV and 1768.2 keV (FEP efficiencies:  $\eta_{1731.7} = 1.84\%$  and  $\eta_{1768.2} = 1.81\%$ ), respectively.

As shown in Fig. 4, in such cases the  $\gamma$ -ray peaks of  $^{214}\text{Bi}$  and  $^{207}\text{Bi}$  are present – in the energy range of interest – in both energy spectra measured with and without the  $\text{Sm}_2\text{O}_3$  sample. However, comparing the counts of each  $\gamma$ -ray peaks measured in the two spectra, we can note that the relative residuals:  $(3.1 \pm 3.6)$ ,  $(-1.1 \pm 5.7)$  and  $(-4.1 \pm 5.1)$  counts for the lines at 1729.6 keV, 1764.5 keV and 1770.2 keV, respectively, are compatible with zero. Therefore, we can be confident that the  $^{214}\text{Bi}$  and  $^{207}\text{Bi}$   $\gamma$ -ray peaks in the energy spectra with the  $\text{Sm}_2\text{O}_3$  sample are due to the intrinsic background of the experimental setup. Thus, the background model for the energy range of the expected peaks is made of a flat component and of the  $^{214}\text{Bi}$  and  $^{207}\text{Bi}$   $\gamma$  peaks; in particular: (i) the contribution of the three peaks is determined from the background data by using a flat component and three

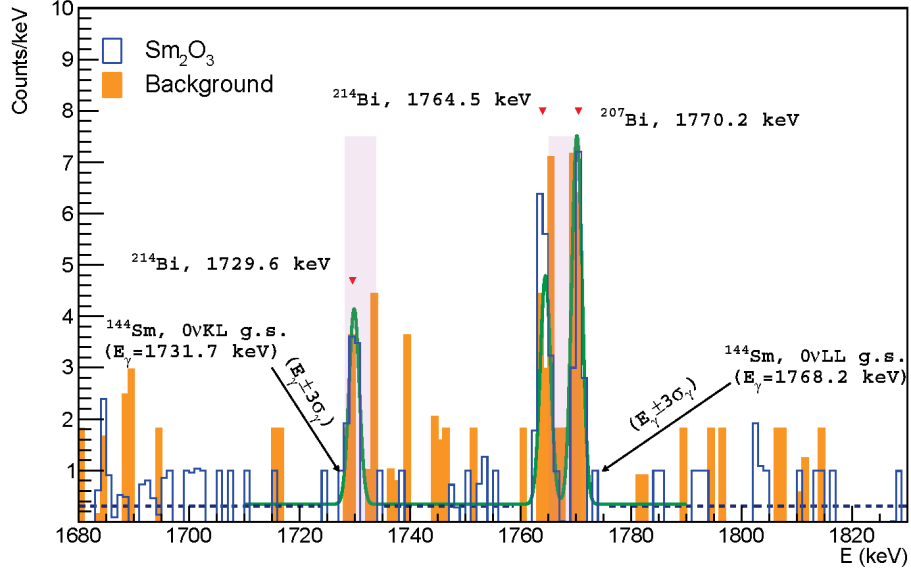


Figure 4: Part of the energy spectrum measured with the  $\text{Sm}_2\text{O}_3$  sample over 1899 h, where the  $\gamma$  peaks from the  $0\nu KL$  and  $0\nu 2L$  processes in  $^{144}\text{Sm}$  to the g.s. of  $^{144}\text{Nd}$  are expected. The fit (green, color on-line) of the background data (a straight line plus the 1729.6 keV and 1764.5 keV Gaussian  $\gamma$  peaks from  $^{214}\text{Bi}$  and 1770.2 keV peak from  $^{207}\text{Bi}$ ) is shown. The constant fit (dashed blue on-line) of the data with the  $\text{Sm}_2\text{O}_3$   $6\sigma$  far from the mentioned  $\gamma$ -ray peaks of  $^{214}\text{Bi}$  and  $^{207}\text{Bi}$  is also reported. The boxes (transparent pink on-line) indicate the energy range ( $E_\gamma \pm 3\sigma_\gamma$ ) expected for the  $0\nu KL$  and  $0\nu 2L$  decay processes to the g.s. of  $^{144}\text{Nd}$  in the energy spectra measured with the  $\text{Sm}_2\text{O}_3$  sample (see text).

Gaussian functions (green on-line in the Fig. 4); (ii) the flat component in the samarium spectrum is evaluated by fitting of the samarium spectrum with a straight line, excluding  $6\sigma$  from the  $^{214}\text{Bi}$  and  $^{207}\text{Bi}$  peaks (dashed blue on-line in Fig. 4). The energy range of interest, used for this analysis, is  $E_\gamma \pm 3\sigma_\gamma$ , where  $E_\gamma$  are the energy of the  $\gamma$  quanta expected for the  $0\nu KL$  and  $0\nu 2L$  decays to the g.s. of  $^{144}\text{Nd}$  (pink transparent boxes on-line in Fig. 4). Here, using the described background model, one can estimate the residual counts for the  $0\nu KL$  and  $0\nu 2L$  decays to the g.s. of  $^{144}\text{Nd}$ :  $(-1.3 \pm 4.4)$  and  $(-2.4 \pm 5.6)$  counts, respectively. According to the procedure of Ref. [55], the

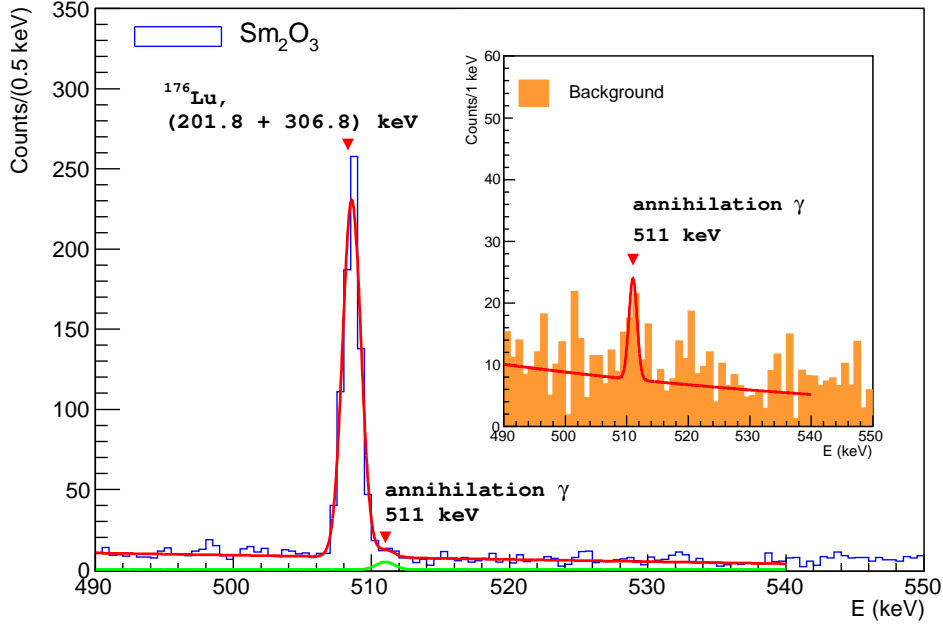


Figure 5: Energy spectrum measured with the samarium oxide sample over 1899 h and background spectrum (inset frame) measured over 1046 h in the vicinity of the 511 keV annihilation peak (the red – colored on-line – line in the inset frame is the fit of the background data). In the  $\text{Sm}_2\text{O}_3$  sample the 508.6 keV peak belonging to  $^{176}\text{Lu}$  is also present. The fit of the  $\text{Sm}_2\text{O}_3$  sample data takes into account the 511 keV  $\gamma$  quanta (green on-line) and the 508.6 keV peak of  $^{176}\text{Lu}$ . The red (colored on-line) line in the main figure is the total fit of  $\text{Sm}_2\text{O}_3$  sample (see text).

derived  $S_{lim}$  values are 6.0 counts and 7.0 counts, respectively. Thus, the following half-life limits are obtained:  $T_{1/2} \geq 1.7 \times 10^{19}$  yr and  $T_{1/2} \geq 1.4 \times 10^{19}$  yr, respectively.

One positron is expected in the  $2\nu\epsilon\beta^+$  ( $0\nu\epsilon\beta^+$ ) decay of  $^{144}\text{Sm}$  with an energy up to 761 keV. The annihilation of the positron should produce two 511 keV  $\gamma$  quanta resulting in an extra counting rate in the annihilation peak. To estimate the  $S_{lim}$  value, the energy spectra accumulated with the  $\text{Sm}_2\text{O}_3$  sample and the background data were fitted in the energy interval (490–540) keV; the fit of the  $\text{Sm}_2\text{O}_3$  sample data takes into account also the 508.6 keV peak of  $^{176}\text{Lu}$  (see Fig. 5). Considering the area of the annihilation peak in the background, in the data accumulated with the samarium oxide sample

there are  $(-11 \pm 12)$  residual events in the 511 keV peak. Since there is no evidence of the effect searched for, we derive  $S_{lim} = 10$  counts. The FEP efficiencies for the  $0\nu\epsilon\beta^+$  and  $2\nu\epsilon\beta^+$  processes are very similar (see Table 4). The obtained half-life limits for the transition to the g.s are  $3.5 \times 10^{19}$  yr and  $3.6 \times 10^{19}$  yr, respectively, while for the transition to the  $2^+$  696.6 keV level of  $^{144}\text{Nd}$  the half-life limit  $3.2 \times 10^{19}$  yr is obtained in both cases.

## 2.5 Search for $2\beta^-$ processes in $^{154}\text{Sm}$

The double beta decay of  $^{154}\text{Sm}$  is possible to the ground state and to the excited levels of  $^{154}\text{Gd}$  with energy 123.1 keV, 680.7 keV, 815.5 keV, 996.3 keV and 1182.1 keV (see Fig. 2). Our experiment is sensitive only to the transition to excited levels.

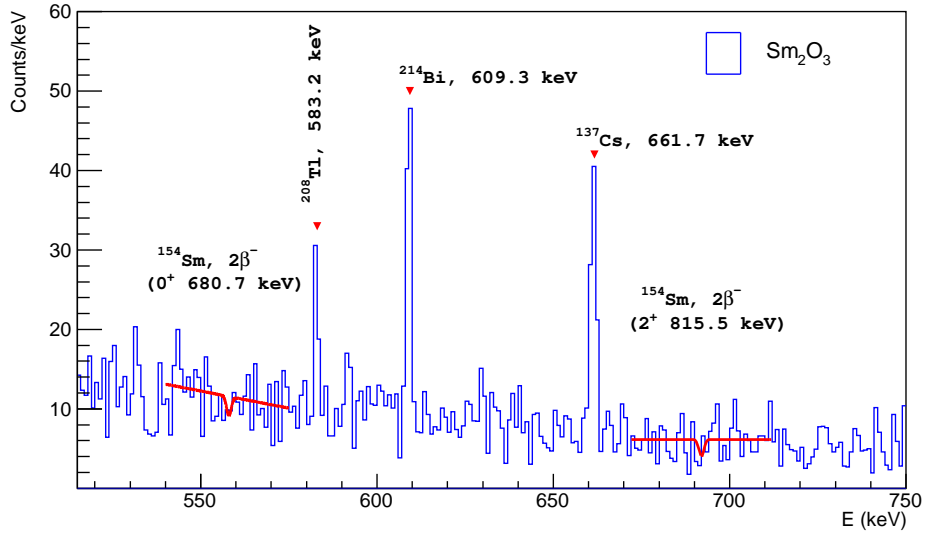


Figure 6: Part of the energy spectrum measured with the  $\text{Sm}_2\text{O}_3$  sample over 1899 h, where the  $\gamma$ -ray peaks from the  $2\beta^-$  in  $^{154}\text{Sm}$  to the  $0^+$  680.7 keV and  $2^+$  815.5 keV excited levels of the  $^{154}\text{Gd}$  are expected. The fits are shown by solid (red on-line) lines; the energy ranges of the fits are (540–575) keV and (672–712) keV.

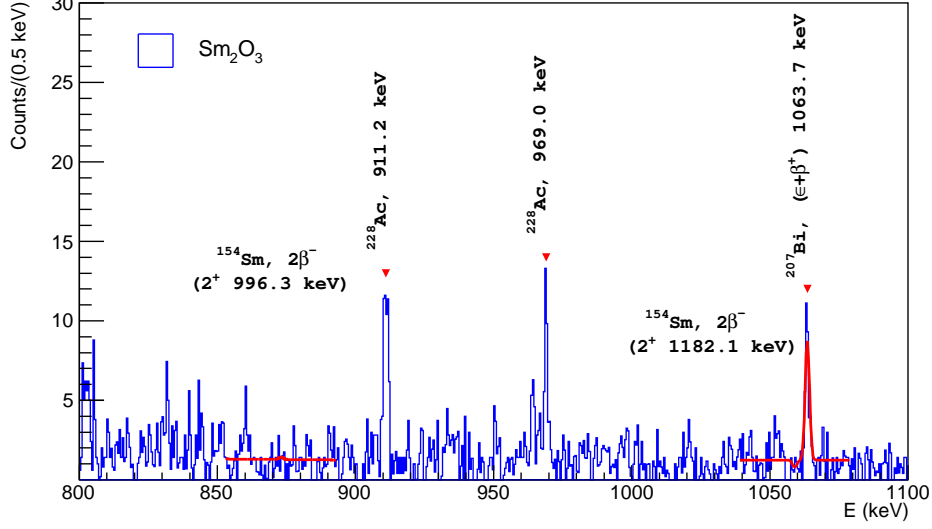


Figure 7: Part of the energy spectrum accumulated with the  $\text{Sm}_2\text{O}_3$  sample over 1899 h, where the  $\gamma$ -ray peaks from the  $2\beta^-$  in  $^{154}\text{Sm}$  to  $2^+$  996.3 keV and  $0^+$  1182.1 keV excited levels of  $^{154}\text{Gd}$  are expected. The fits are shown by solid (red on-line) lines. The energy range of the fits are (853–893) keV and (1039–1079) keV.

As regards the transition to the first excited level at 123.1 keV, the energy spectrum acquired with the samarium oxide sample was fitted in the energy interval (110–135) keV by a model consisting of a Gaussian function centered at 123.1 keV (to describe the effect searched for) and a straight line as a background model. The fit gives an area of the 123.1 keV peak equal to  $(11 \pm 10)$  counts; thus, there is no evidence for the effect searched for. Therefore, according to Ref. [55], we derive  $S_{lim} = 27$  counts. Taking into account the number of  $^{154}\text{Sm}$  nuclei in the sample, and the FEP detection efficiency  $\eta = 0.40\%$ , we have obtained the limit on the  $2\beta^-$  decay of  $^{154}\text{Sm}$  to the first  $2^+$  excited level of  $^{154}\text{Gd}$ :  $T_{1/2} \geq 6.0 \times 10^{18}$  yr. This limit is for the sum of the  $2\nu 2\beta^-$  and  $0\nu 2\beta^-$  modes, since they cannot be distinguished with the  $\gamma$ -spectrometry method.

As regards the other excited levels of the  $^{154}\text{Gd}$ , 680.7 keV, 815.5 keV,

996.3 keV, 1182.1 keV de-excitation gamma peaks are expected at 557.6 keV, 692.4 keV, 873.2 keV and 1059.0 keV, respectively (see Fig. 2). The spectrum in the vicinity of the expected peaks is shown in Figs. 6 and 7. In the first three cases the energy spectrum with the  $\text{Sm}_2\text{O}_3$  sample was fitted by the sum of a Gaussian function (to describe the peak searched for) and of a straight line to describe the background.

In the case of the  $2\beta^-$  decay to the 1182.1 keV level of  $^{154}\text{Nd}$ , also the 1063.7 keV peak of  $^{207}\text{Bi}$  was included in the fit to approximate the background in a large enough energy interval around the peak searched for (see Fig. 7). To perform the fits, the energy range was fixed for these 4 cases as: (540–575) keV, (672–712) keV, (853–893) keV and (1039–1079) keV, respectively. The results of the fits give for the effects searched for the values:  $(-4.1 \pm 5.1)$ ,  $(-3.7 \pm 3.3)$ ,  $(0.3 \pm 1.5)$ ,  $(-0.9 \pm 1.1)$  counts, respectively. According to the procedure given in Ref. [55], the corresponding  $S_{lim}$  values are 4.8, 2.4, 2.8 and 1.0 counts, respectively; thus, the half-life limits are in the range  $T_{1/2} \geq (2.0 - 8.0) \times 10^{20}$  yr (see Table 4).

### 3 Conclusions

A method of samarium purification from radioactive contaminants in traces, based on the liquid-liquid extraction was performed. In particular, traces of  $^{40}\text{K}$ ,  $^{137}\text{Cs}$  and  $^{226}\text{Ra}$  were observed in the purified  $\text{Sm}_2\text{O}_3$  sample at the level of  $\sim(1 - 10)$  mBq/kg, while other contaminants – as e.g.  $^{228}\text{Th}$  – are below the experimental sensitivity of  $\sim 1$  mBq/kg. Instead the adopted protocol of samarium purification is not effective for the segregation of  $^{176}\text{Lu}$ . Further investigations are in progress.

The  $2\epsilon$  and  $\epsilon\beta^+$  decay modes in  $^{144}\text{Sm}$ , and the  $2\beta^-$  of  $^{154}\text{Sm}$  to the excited levels  $2^+$  or  $0^+$  of  $^{154}\text{Gd}$  were searched for using 342 g of a highly purified  $\text{Sm}_2\text{O}_3$  sample and the ultra-low background HP-Ge  $\gamma$  spectrometer at the STELLA facility of the Gran Sasso National Laboratory. For the first time, limits on the different decay modes and channels of double beta decay of  $^{154}\text{Sm}$  and  $^{144}\text{Sm}$  were set at a level of  $T_{1/2} > 10^{18} - 10^{20}$  yr. This sensitivity is not so far from those of the most sensitive  $2\beta^+$  experiments, which are typically at a level of  $T_{1/2} \sim 10^{21} - 10^{22}$  yr [24, 25, 56–68]. The  $T_{1/2}$  limits, obtained in this work, for the  $^{144}\text{Sm}$   $2\epsilon$  and  $\epsilon\beta^+$  processes are 10 – 11 orders of magnitude higher than those recently derived in Ref. [40].



## 4 Acknowledgments

The group from the Institute for Nuclear Research (Kyiv, Ukraine) was supported in part by the program of the National Academy of Sciences of Ukraine “Fundamental research on high-energy physics and nuclear physics” (international cooperation). O.G.P. was supported in part by the project “Investigations of rare nuclear processes” of the program of the National Academy of Sciences of Ukraine “Laboratory of young scientists” (Grant No. 0118U002328).

## References

- [1] J. Barea et al., Phys. Rev. Lett. 109 (2012) 042501.
- [2] W. Rodejohann, J. Phys. G 39 (2012) 124008.
- [3] F.F. Deppisch et al., J. Phys. G 39 (2012) 124007.
- [4] S.M. Bilenky et al., Int. J. Mod. Phys. A 30 (2015) 1530001.
- [5] S. Dell’Oro et al., AHEP 2016 (2016) 2162659.
- [6] J.D. Vergados et al., Int. J. Mod. Phys. E 25 (2016) 1630007.
- [7] V.I. Tretyak et al., At. Data Nucl. Data Tables 80 (2002) 83.
- [8] S.R. Elliott, Mod. Phys. Lett. A 27 (2012) 123009.
- [9] A. Giuliani et al., AHEP 2012 (2012) 857016.
- [10] O. Cremonesi et al., AHEP 2014 (2014) 951432.
- [11] X. Sarazin, J. Phys.: Conf. Ser. 593 (2015) 012006.
- [12] R. Arnold et al., Phys. Rev. D 92 (2015) 072011.
- [13] A. Gando et al., Phys. Rev. Lett. 117 (2016) 082503.
- [14] J.B. Albert et al., Phys. Rev. Lett. 120 (2018) 072701.
- [15] C. Alduino et al., Phys. Rev. Lett. 120 (2018) 132501.

- [16] C.E. Aalseth et al., Phys. Rev. Lett. 120 (2018) 132502.
- [17] M. Agostini et al., Phys. Rev. Lett. 120 (2018) 132503.
- [18] O. Azzolini et al., Phys. Rev. Lett. 120 (2018) 232502.
- [19] J. Maalampi et al., AHEP 2013 (2013) 505874.
- [20] M. Hirsch et al., Z. Phys. A 347 (1994) 151.
- [21] R. Winter et al., Phys. Rev. 100 (1955) 142.
- [22] M.B. Voloshin et al., JETP Lett. 35 (1982) 656.
- [23] J. Bernabeu et al., Nucl. Phys. B 223 (1983) 15.
- [24] K. Blaum et al., Double-Electron Capture, to be submitted to Rev. Mod. Phys.
- [25] M.I. Krivoruchenko et al., Nucl. Phys. A 859 (2011) 140.
- [26] M. Georgi et al., Nucl. Phys. B 193 (1981) 297.
- [27] S.A. Eliseev et al., J. Phys. G. 39 (2012) 124003.
- [28] R. Saakyan, Annu. Rev. Nucl. Part. Sci. 63 (2013) 503.
- [29] A.A. Sonzogni, Nucl. Data Sheets 93 (2001) 599.
- [30] C. W. Reich, Nucl. Data Sheets 110 (2009) 2257.
- [31] M. Wang et al., Chin. Phys. C 41 (2017) 030003.
- [32] J. Meija et al., Pure Appl. Chem. 88 (2016) 293.
- [33] P. Belli et al., Nucl. Phys. A 930 (2014) 195.
- [34] P. Belli et al., Nucl. Phys. A 990 (2019) 64.
- [35] A.S. Barabash et al., Nucl. Phys. At. Energy 19 (2018) 95.
- [36] P. Belli et al., J. Phys. G 45 (2018) 095101.
- [37] P. Belli et al., Eur. Phys. J. A 53 (2017) 172.

- [38] R.S. Boiko, Int. J. Mod. Phys. A 32 (2017) 1743005.
- [39] Z. Sujkowski et al., Phys. Rev. C 70 (2004) 052501.
- [40] F. Nozzoli, Phys. Rev. C 97 (2018) 015501.
- [41] J.G. Hirsch et al., Phys. Lett. B 534 (2002) 57.
- [42] J. Barea et al., Phys. Rev. Lett. 109 (2012) 042501.
- [43] J. Barea et al., Phys. Rev. C 87 (2013) 014315.
- [44] F. Iachello et al, Nucl. Part. Phys. Proc. 265 (2015) 25.
- [45] A.A. Raduta et al., Phys. Rev. C 69 (2004) 064321.
- [46] B. Pritychenko, arXiv:1004.3280 [nucl-th].
- [47] C.M. Raduta et al., Phys. Rev. C 84 (2011) 064322.
- [48] Y.J. Ren et al., Phys. Rev. C 89 (2014) 064603.
- [49] V.I. Tretyak, Yu.G. Zdesenko, At. Data Nucl. Data Tables 61 (1995) 43.
- [50] A.V. Derbin et al., Phys. At. Nucl. 59 (1996) 2037.
- [51] P. Belli et al., Eur. Phys. J. A 53 (2017) 172.
- [52] P. Belli et al., Nucl. Phys. A 859 (2011) 126.
- [53] I. Kawrakow, D.W.O. Rogers, NRCC Report PIRS-701, Ottawa, 2003.
- [54] O.A. Ponkratenko et al., Phys. At. Nucl. 63 (2000) 1282.
- [55] G. J. Feldman and R. D. Cousins, Phys. Rev. D 57 (1998) 3873.
- [56] A.P. Meshik et al., Phys. Rev. C 64 (2001) 035205.
- [57] M. Pujol et al., Geochim. Cosmochim. Acta 73 (2009) 6834.
- [58] Yu.M. Gavriluk et al., Phys. Rev. C 87 (2013) 035501.
- [59] S.S. Ratkevich et al., Phys. Rev. C 96 (2017) 065502.
- [60] M. Agostini et al., Eur. Phys. J. C 76 (2016) 652.

- [61] G. Angloher et al., J. Phys. G 43 (2016) 095202.
- [62] B. Lehnert et al., J. Phys. G 43 (2016) 065201.
- [63] P. Belli et al., J. Phys. G 38 (2011) 115107.
- [64] P. Belli et al., Phys. Rev. C 87 (2013) 034607.
- [65] P. Belli et al., Phys. Rev. C 93 (2016) 045502.
- [66] A.S. Barabash et al., Phys. Rev. C 83 (2011) 045503.
- [67] E. Andreotti et al., Astropart. Phys. 34 (2011) 643.
- [68] Yu.M. Gavriluk et al., Phys. At. Nucl. 78 (2015) 1563.